Supporting Information

Gold Nanoclusters/Iron Oxyhydroxide Platform for Ultrasensitive Detection of Butyrylcholinesterase

Xiao-Ping Zhang, Chen-Xi Zhao, Yang Shu* and Jian-Hua Wang*

Department of Chemistry, College of Sciences, Northeastern University, Box 332, Shenyang 110819, China.

**E-mail:* shuyang@mail.neu.edu.cn; jianhuajrz@mail.neu.edu.cn.

Table of contents

Experimental

Materials and Chemicals

$CoCl_2 \cdot 6H_2O$, $FeCl_3 \cdot 6H_2O$, $Ni(Ac)_2$, polyvinyl pyrrolidone (PVP), urea, sodium hydroxide (NaOH), sodium hypochlorite (NaClO), Chloroauric acid hydrate ($HAuCl_4 \cdot 4H_2O$), hydrochloric acid (HCl) and folic acid were purchased from Aladdin Reagent Co., Ltd. (Shanghai, China). Other anionic salts were obtained from Sinopharm Chemical Reagent Co. (Beijing, China). Butyrylcholinesterase (BChE) from equine serum, acetylthiocholine iodide (ATCh), tacrine and N-ethylmaleimide were purchased from Sigma-Aldrich Co. Ltd (Shanghai, China). All the reagents were used as received without further purification. Ultrapure water of 18.2 MΩ·cm was used to prepare all the solutions.

Instrumentation

X-ray diffraction (XRD) patterns were collected on an X'Pert Pro (PANalytical BV, Holland) diffraction meter with Cu Kα, λ = 0.154 nm. The morphology of products were observed using G20 transmission electron microscope (FEI, USA). Fourier transform infrared spectra were recorded by using a Nicolet-6700 FT-IR spectrophotometer (Thermoelectro, USA). X-ray photoelectron spectroscopy (XPS) spectra were recorded on an ESCALAB 250 surface analysis system (Thermo Scientific, USA). Fluorescence was recorded on an F-7000 fluorescence spectrophotometer (Hitachi High-Technologies Corporation, Japan) equipped with a quartz cell (Optical path: 4×4 mm).

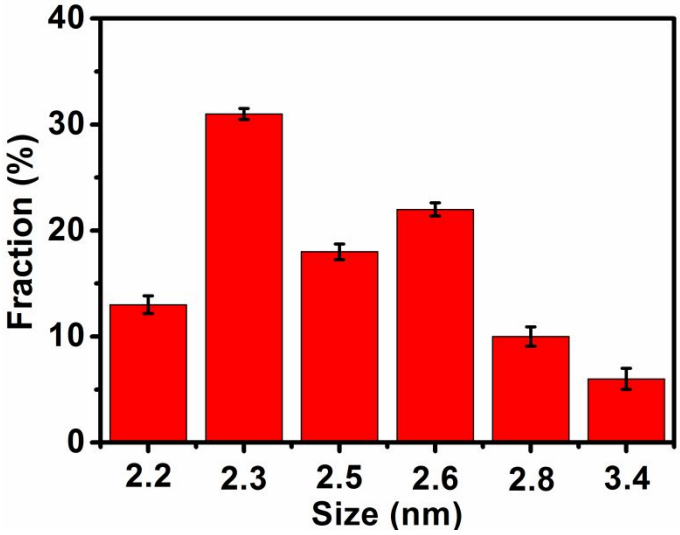

Figure S1. Hydrodynamic size distribution of AuNCs in aqueous medium.

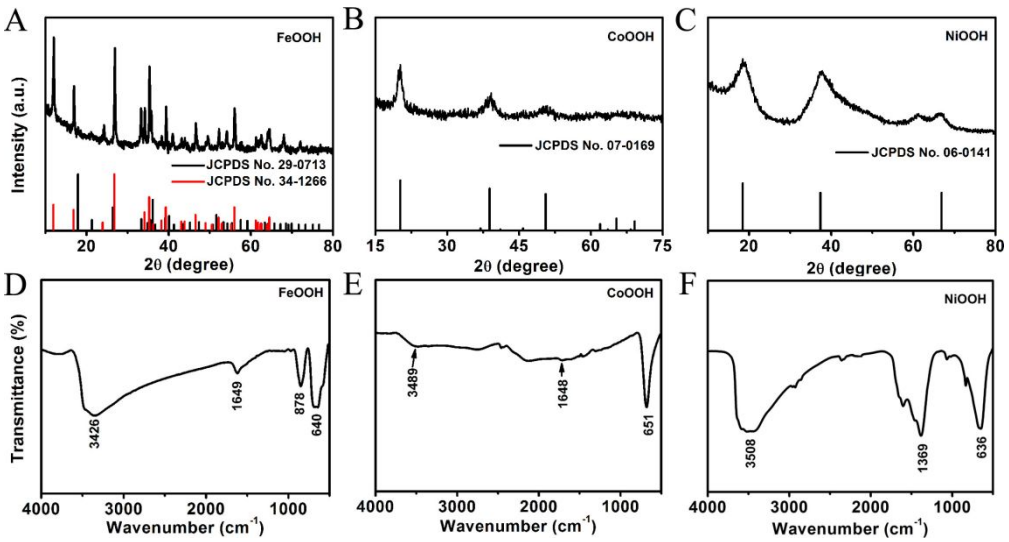

Figure S2. XRD patterns for (A) FeOOH nanorods, (B) CoOOH nanosheets, and (C) NiOOH nanoflakes. FT-IR spectra of (D) FeOOH nanorods, (E) CoOOH nanosheets, and (F) NiOOH nanoflakes.

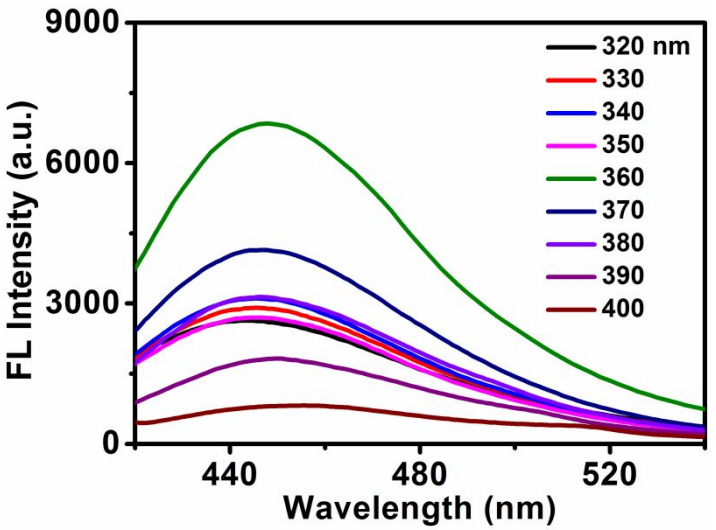

Figure S3. Fluorescence emission spectra for 0.2 mg mL^{-1} of the AuNCs at various excitation wavelength within the range of 320-400 nm.

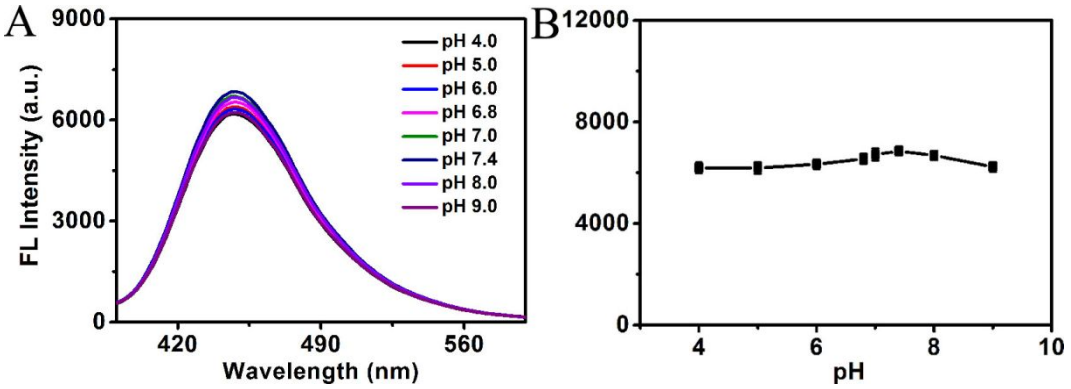

Figure S4. Fluorescence spectra (A) and fluorescence intensity (B) for 0.2 mg mL^{-1} of AuNCs under different pH (pH 4.0-9.0) at λ_{ex}=360 nm.

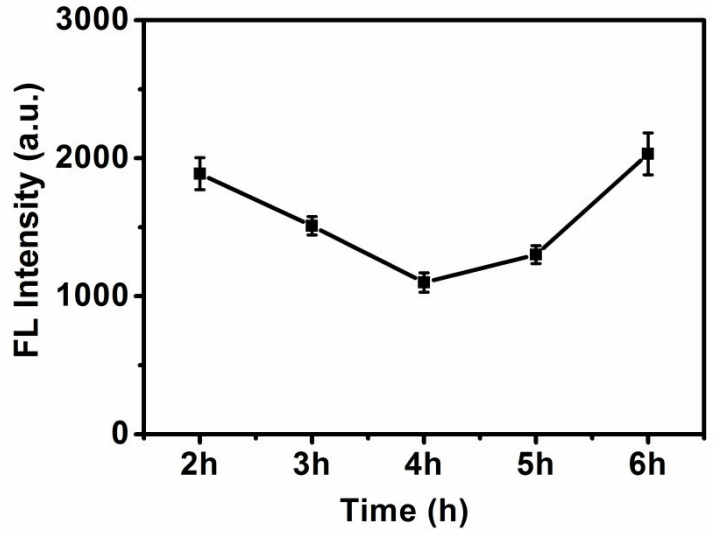

Figure S5. Fluorescence intensity of Au/FeOOH toward various hydrothermal preparation time of FeOOH nanomaterial at λ_{ex}=360 nm (AuNCs: 0.2 mg mL^{-1}, FeOOH: 0.15 mg mL^{-1}).

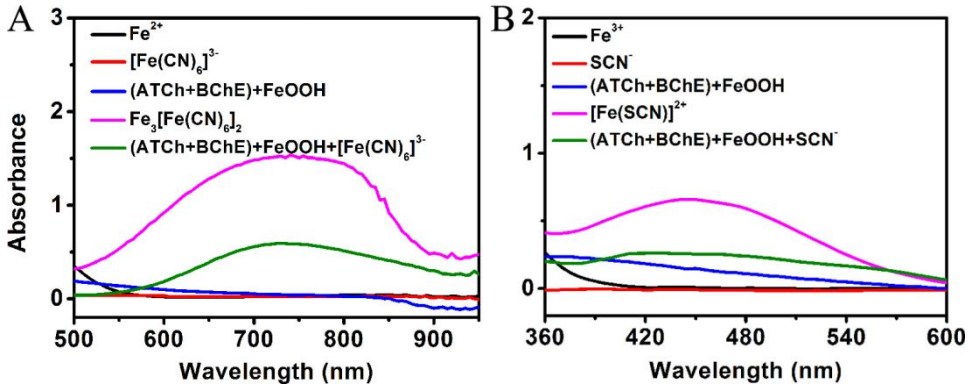

Figure S6. UV-vis absorption spectra of (A) 30 mmol L^{-1} of Fe^{2+}, 20 mmol L^{-1} of $[Fe(CN)_6]^{3-}$, (ATCh+BChE)+FeOOH, 1 mmol L^{-1} of $Fe_3[Fe(CN)_6]_2$, (ATCh+BChE)+FeOOH+$[Fe(CN)_6]^{3-}$, and (B) 50 mmol L^{-1} of Fe^{3+}, 50 mmol L^{-1} of SCN^-, (ATCh+BChE)+FeOOH, 5 mmol L^{-1} of $[Fe(SCN)]^{2+}$, (ATCh+BChE)+FeOOH+ SCN^-. (ATCh: 100 mmol L^{-1}, BChE: 1 mg mL^{-1}, FeOOH: 0.15 mg mL^{-1}).

The specific reaction between Fe^{2+} and $[Fe(CN)_6]^{3-}$ is given below:

$3\ Fe^{2+} + 2\ [Fe(CN)_6]^{3-} \rightarrow Fe_3[Fe(CN)_6]_2$ (blue precipitate)

The specific reaction between Fe^{3+} and SCN^- is given below:

$Fe^{3+} + SCN^- \rightarrow [Fe(SCN)]^{2+}$ (blood red)

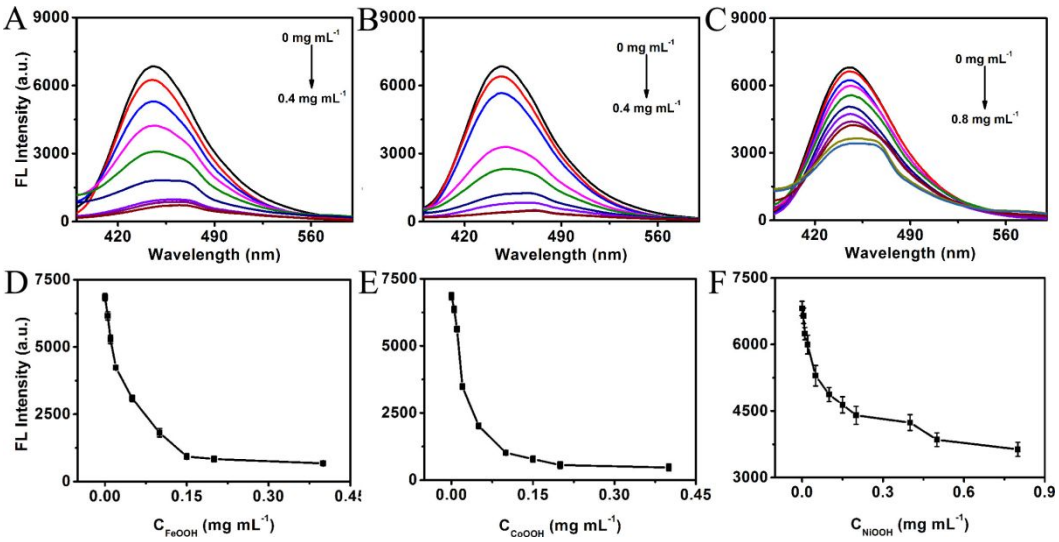

Figure S7. Fluorescence spectra of Au/MOOH for (A) FeOOH, (B) CoOOH, and (C) NiOOH, and fluorescence intensity of AuNCs toward different concentrations of (D) FeOOH, (E) CoOOH, and (F) NiOOH, at λ_{ex}=360 nm, respectively (AuNCs: 0.2 mg mL^{-1}).

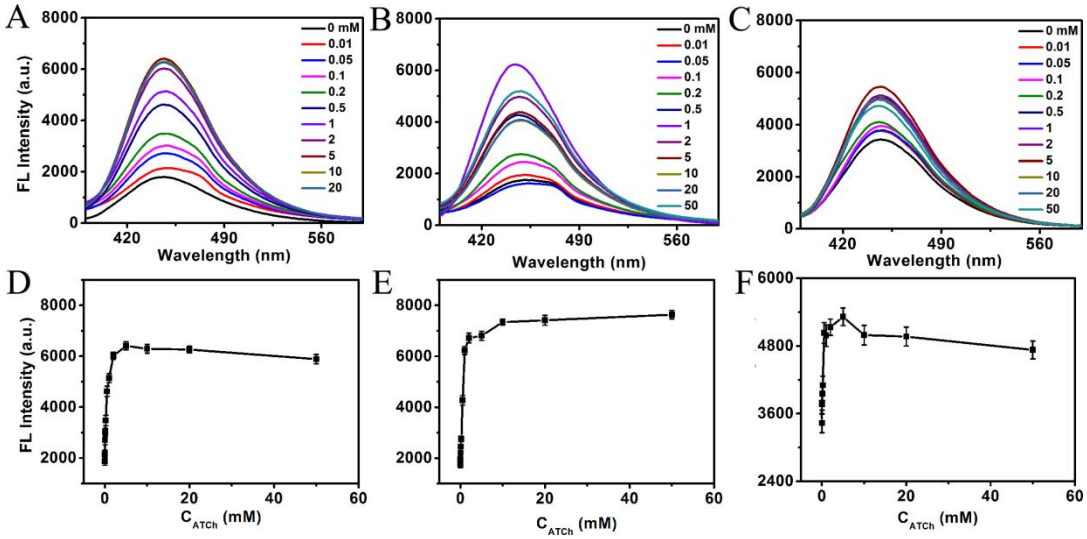

Figure S8. Fluorescence spectra with various concentrations of ATCh for (A) 0.15 mg mL^{-1} of FeOOH, (B) 0.2 mg mL^{-1} of CoOOH, and (C) 0.5 mg mL^{-1} of NiOOH, and the corresponding curves for (D) FeOOH, (E) CoOOH, and (F) NiOOH, at λ_{ex}=360 nm, respectively.

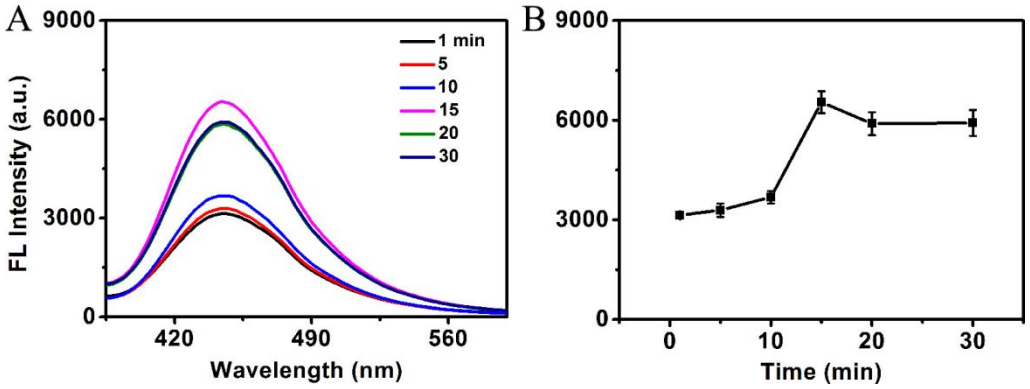

Figure S9. Fluorescence spectra (A) and fluorescence intensity (B) with various reaction times of ATCh and BChE, at λ_{ex}=360 nm.

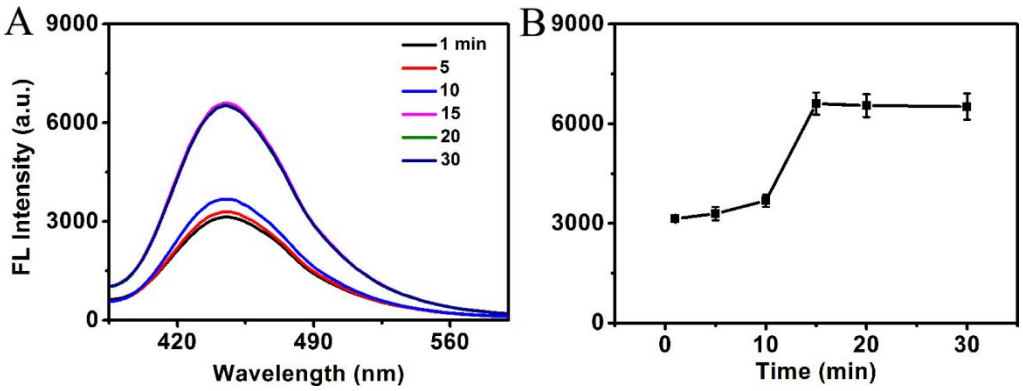

Figure S10. Fluorescence spectra (A) and fluorescence intensity (B) with various reaction times for the enzymatic hydrolysate with FeOOH, at λ_{ex}=360 nm.

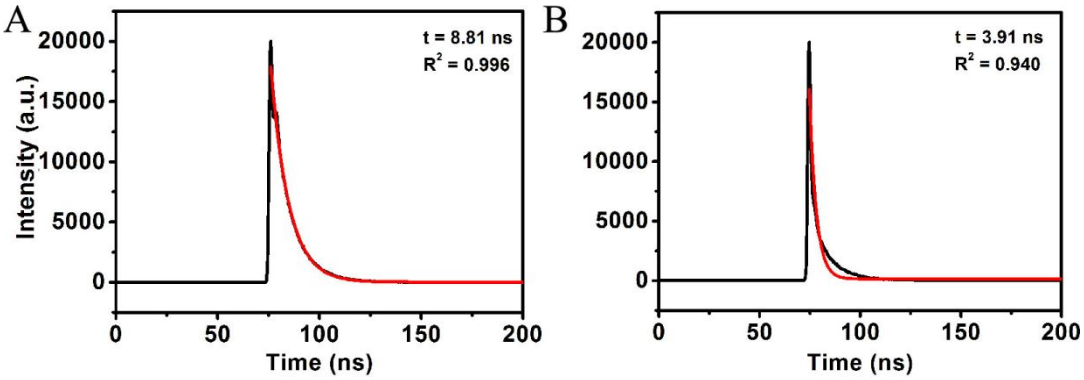

Figure S11. Decay curves of AuNCs in the (A) absence and (B) presence of FeOOH nanomaterials, at λ_{ex}=360 nm.

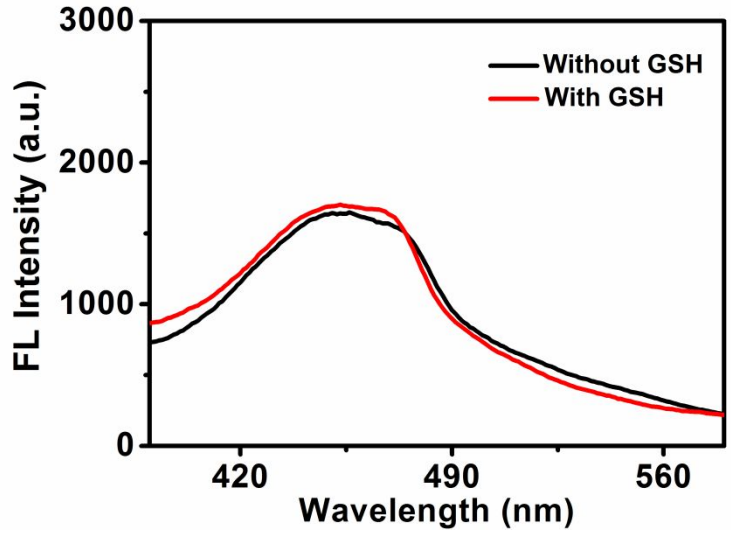

Figure S12. Fluorescence intensity in the presence and in the absence of GSH at λ_{ex}=360 nm (AuNCs: 0.2 mg mL^{-1}, FeOOH: 0.15 mg mL^{-1}, GSH: 3.8 ng mL^{-1}).

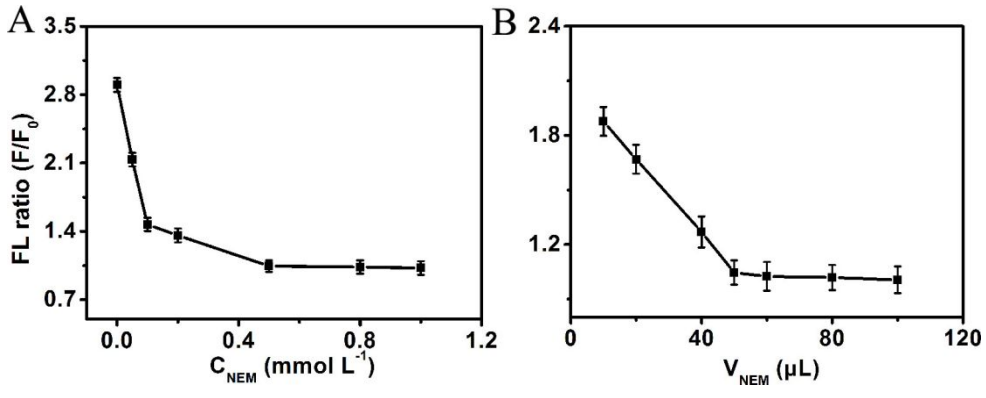

Figure S13. The dependence of fluorescence ratio (F/F_0) on (A) NEM concentration and (B) NEM volume at λ_{ex}=360 nm (AuNCs: 0.2 mg mL^{-1}, FeOOH: 0.15 mg mL^{-1}).

Table S1. Comparison of the present assay protocol for BChE with the reported methods

Method	LOD ($\mu g\ mL^{-1}$)	RSD	Ref.
Ellman's colorimetry	—	4.8%	1
Radiochemical	—	—	2
Velocity	0.68	1.7%	3
MALDI-TOF-MS	—	—	4
Electrochemistry	25.0	3.2%	5
Colorimetry	0.15	—	6
Colorimetry	2	3.6%	7
Enzyme-linked immunosorbent assay	0.03	—	8
Electrochemical assay	0.03	—	9
Potentiometric assay	0.2	—	10
Fluorescence (CQDs-Cu^{2+})	1.06	—	11
Fluorescence (MGA-QDs)	2.5	—	12
Fluorescence (CDs-OPD)	0.04	2.2%	13
Fluorescence (BChE-FP)	—	—	14
Fluorescence (CQDs-Au)	—	—	15
Fluorescence (FeOOH)	0.004	2.3%	
Fluorescence (CoOOH)	0.01	1.7%	This work
Fluorescence (NiOOH)	0.07	3.4%	

Table S2. BChE determination in finger blood, whole blood, plasma with the Au/FeOOH fluorescence probe

Measured BChE concentration	Sample	Au/FeOOH probe (mg mL^{-1})	Mean (mg mL^{-1})	RSD (%) (n = 5)
Finger blood	1	2.12 ± 0.121	2.21	3.91
	2	2.28 ± 0.107		
	3	2.23 ± 0.142		
Whole blood	1	2.18 ± 0.132	2.25	2.71
	2	2.33 ± 0.115		
	3	2.25 ± 0.204		
Plasma	1	2.35 ± 0.188	2.35	2.32
	2	2.28 ± 0.146		
	3	2.41 ± 0.159		

Table S3. The recovery of BChE in finger blood, human whole blood, and plasma with the Au/FeOOH fluorescence probe

Sample	Spiked ($ng\ mL^{-1}$)	Found ($ng\ mL^{-1}$)	Recovery (%)	RSD (%) (n = 3)
Finger blood	0	21.3 ± 3	—	—
	40	60.2 ± 1	98.2	3.03
	80	99.8 ± 3	98.5	2.98
Whole blood	0	22.1 ± 2	—	—
	40	61.3 ± 1	98.4	1.92
	80	104 ± 3	102	3.50
Plasma	0	23.5 ± 3	—	—
	40	60.1 ± 4	96.8	2.91
	80	101 ± 2	99.1	3.04

References

(1) Ellman, G. L.; Courtney, K. D.; Andres, V.; Featherstone, R. M. A new and rapid colorimetric determination of acetylcholinesterase activity. *Biochem. Pharmacol.* **1961**, *7*, 88−95.

(2) Winteringham, F. P. W.; Disney, R. W. Radiometric assay of acetylcholinesterase. *Nature* **1962**, *195*, 1303.

(3) Chen, G.; Feng, H.; Jiang, X.; Xu, J.; Pan, S.; Qian, Z. Redox-controlled fluorescent nanoswitch based on reversible disulfide and its application in butyrylcholinesterase activity assay. *Anal. Chem.* **2018**, *90*, 1643−1651.

(4) Hu, L.; Jiang, G.; Xu, S.; Pan, C.; Zou, H. Monitoring enzyme reaction and screening enzyme inhibitor based on MALDI-TOF-MS platform with a matrix of oxidized carbon nanotubes. *J. Am. Soc. Mass. Spectr.* **2006**, *17*, 1616−1619.

(5) Panraksa, Y.; Siangproh, W.; Khampieng, T.; Chailapakul, O.; Apilux, A. based amperometric sensor for determination of acetylcholinesterase using screen-printed graphene electrode. *Talanta* **2018**, *178*, 1017−1023.

(6) Wang, M.; Gu, X.; Zhang, G.; Zhang, D.; Zhu, D. Continuous colorimetric assay for acetylcholinesterase and inhibitor screening with gold nanoparticles. *Langmuir* **2009**, *25*, 2504−2507.

(7) Liu, C.; Gomez, F. A. A microfluidic paper‐based device to assess acetylcholinesterase activity. *Electrophoresis* **2017**, *38*, 1002−1006.

(8) Wang, L.; Du, D.; Lu, D.; Lin, C.; Smith, J.; Timchalk, C.; Liu, F.; Wang, J.; Lin, Y. Enzyme-linked immunosorbent assay for detection of organophosphorylated butyrylcholinesterase: A biomarker of exposure to organophosphate agents. *Anal. Chim. Acta* **2011**, *693*, 1−6.

(9) Lu, D.; Wang, J.; Wang, L.; Du, D.; Timchalk, C.; Barry, R.; Lin, Y. A novel nanoparticle‐based disposable electrochemical immunosensor for diagnosis of exposure to toxic organophosphorus agents. *Adv. Funct. Mater.* **2011**, *21*, 4371−4378.

(10) Khaled, E.; Hassan, H. N.; Mohamed, G. G.; Ragab, F. A.; Seleim, A. E. Disposable potentiometric sensors for monitoring cholinesterase activity. *Talanta* **2010**, *83*, 357−363.

(11) Qian, Z.; Chai, L.; Tang, C.; Huang, Y.; Chen, J.; Feng, H. A fluorometric assay for acetylcholinesterase activity and inhibitor screening with carbon quantum dots. *Sens. Actuators B-Chem.* **2016**, *222*, 879−886.

(12) Chen, Z.; Ren, X.; Meng, X.; Tan, L.; Chen, D.; Tang, F. Quantum dots-based fluorescent probes for turn-on and turn-off sensing of butyrylcholinesterase. *Biosens. Bioelectron.* **2013**, *44*, 204−209.

(13) Xu, X.; Cen, Y.; Xu, G.; Wei, F.; Shi, M.; Hu, Q. A ratiometric fluorescence probe based on carbon dots for discriminative and highly sensitive detection of acetylcholinesterase and butyrylcholinesterase in human whole blood. *Biosens. Bioelectron.* **2019**, *131*, 232−236.

(14) Yang, S.; Sun, Q.; Xiong, H.; Liu, S.; Moosavi, B.; Yang, W.; Yang, G. Discovery of a butyrylcholinesterase-specific probe via a structure-based design strategy. *Chem. Commun.* **2017**, *53*, 3952−3955.

(15) Wu, X.; Song, Y.; Yan, X.; Zhu, C.; Ma, Y.; Du, D.; Lin, Y. Carbon quantum dots as fluorescence resonance energy transfer sensors for organophosphate pesticides determination. *Biosens. Bioelectron.* **2017**, *94*, 292−297.